Materials Horizons

ROYAL SOCIETY OF CHEMISTRY

COMMUNICATION

View Article Online
View Journal | View Issue

Cite this: *Mater. Horiz.*, 2025, 12, 3399

Received 21st December 2024,
Accepted 25th February 2025

DOI: 10.1039/d4mh01876a

rsc.li/materials-horizons

Semiconducting liquid crystalline dispersions with precisely adjustable band gaps and polarized photoluminescence†

Tingting Zhou,[ab] Penghao Guo,[ab] Xuelian Jiang,[ab] Hongbo Zhao,[ab] Qing Zhang[c] and Pei-Xi Wang *[ab]

Simultaneously possessing energy conversion properties and reconfigurable anisotropic structures due to their fluidity, semiconducting liquid crystals are an emerging class of soft materials for generating and detecting polarized photons. However, band-gap engineering of liquid crystalline substances remains challenging. Herein, semiconducting liquid crystals exhibiting discotic nematic ordering, linearly polarized monochromatic photoluminescence or broadband white-light emission, and polarization-dependent light-responsiveness (generation of photons and photocurrents) were systematically developed by transforming two-dimensional organic–inorganic metal halide perovskites into mesogenic colloidal nanoparticles. The emission wavelengths of the perovskite liquid crystals could be adjusted with an accuracy of 5 nanometers over a wide range in the visible region by compositional variations, indicating the possibility of fabricating polarized light-emitting or optoelectronic devices with desired band gaps using these materials.

New concepts

In this study, luminescent liquid crystals with precisely tunable semiconducting bandgaps were synthesized. Simply through elemental doping, the emission wavelengths of these liquid crystals could be adjusted in the visible range with an accuracy of 5 nm, which has not been achieved in the past by other liquid crystalline materials. Liquid crystals emitting red, green, blue, and white light were systematically developed. Owing to their self-assembled anisotropic superstructures and semiconductivity, they could generate polarized light and detect polarized photons by producing polarization-dependent photocurrents. These results suggest a new and low-cost approach to hierarchically structured semiconductors with versatile optical and electronic properties, which may have applications in polarized light sources (*e.g.*, LCD backlights), photodetectors, and robotic imaging systems.

Introduction

The combination of semiconductivity and liquid crystalline structures provides charge-transfer and photon–exciton interaction processes with reconfigurable anisotropic optical and electrical environments, therefore have applications in linearly or circularly polarized light sources,[1–7] photodetectors,[8,9] lasers,[10,11] field-effect transistors,[12–14] and various types of smart optoelectronics.[15,16] Liquid crystals with intrinsic semiconducting properties were mainly developed in two ways: by modifying molecular or colloidal semiconductors with liquid crystalline moieties possessing geometrical anisotropy,[17–23] or by turning semiconductive materials into one-dimensional or two-dimensional anisotropic mesogenic nanoparticles.[24–35] However, due to the limitations from organic synthesis (for molecular mesogens) or morphological control (for colloidal mesogens), it is often not easy to precisely adjust the bandgaps of semiconducting liquid crystals over a wide range. To solve this problem, we considered introducing liquid crystallinity to metal halide perovskites, an emerging type of solution-processable semiconductors.[36–39]

Metal halide perovskites, consisting of corner-sharing metal halide octahedral units and organic ammonium spacer cations, possess excellent compositional and structural diversity as well as tunable semiconducting properties, and therefore have applications in solar cells,[40] light-emitting diodes,[41–43] lasing systems,[44] photodetectors,[45–47] ferroelectrics,[48,49] electro-optical devices,[50] photocatalysis,[51] *etc.* Some attempts have been made to combine liquid crystalline species with perovskites. By using molecular liquid crystals as additives, organic ligands, or templates, perovskite materials with improved photovoltaic or optoelectronic performances might be synthesized.[52–55] In a special case, by incorporating polyfluorinated imidazolium spacer cations in the crystal lattices of hybrid organic–inorganic halide perovskites,

[a] *School of Nano-Tech and Nano-Bionics, University of Science and Technology of China, 96 Jinzhai Road, Hefei, Anhui, 230026, P. R. China*
[b] *I-Lab, Suzhou Institute of Nano-Tech and Nano-Bionics of the Chinese Academy of Sciences, 398 Ruoshui Road, Suzhou Industrial Park, Suzhou, Jiangsu, 215123, P. R. China. E-mail: pxwang2020@sinano.ac.cn*
[c] *NANO-X Vacuum Interconnected Nanotech Workstation, Suzhou Institute of Nano-Tech and Nano-Bionics of the Chinese Academy of Sciences, 385 Ruoshui Road, Suzhou Industrial Park, Suzhou, Jiangsu, 215123, P. R. China*

† Electronic supplementary information (ESI) available. See DOI: https://doi.org/10.1039/d4mh01876a

thermotropic liquid crystallinity was achieved.[56] Nevertheless, lyotropic liquid crystalline phases of metal halide perovskite nanoparticles would still be worth investigating since colloidal mesogens may preserve the intrinsic physical properties of bulk crystals. Compared with other semiconductors that could be turned into liquid crystals, the bandgaps of perovskites can be accurately adjusted from near-ultraviolet to near-infrared by structural modulation and elemental doping, based on which a large family of semiconducting liquid crystals with different emission wavelengths and other desired electrical/magnetic properties might be systematically developed.

In this research, through microcrystallization processes induced by anti-solvents (solvents miscible with the primary solvent but could not dissolve the perovskite precursors) and facilitated by surfactants, lead(II)- and manganese(II)-based two-dimensional organic–inorganic metal halide perovskites $(R\text{-}NH_3)_2MX_4$ were transformed into colloidal lyotropic liquid crystalline dispersions in nonpolar solvents, where the organic ligands $R\text{-}NH_3$ ranged from aliphatic to aromatic ammonium cations with diverse molecular lengths, and the halide anions X could be chloride, bromide, iodide, or their mixtures. Moreover, lead(II) halide perovskite liquid crystals exhibited polarized photoluminescence and polarization-dependent photon-detection features characteristic of their direct semiconducting bandgaps and structural orderliness (Fig. 1). These results suggest a new way to combine highly-tunable semiconductivity with the versatile light-manipulation abilities of self-assembled ordered superstructures, which may help develop polarized optoelectronic or light-emitting devices.

Results and discussion

Preparation of colloidal nanoplatelets of metal halide perovskites

The synthesis of liquid crystalline mesogens was carried out with a series of organic–inorganic metal halide perovskites including bis(*n*-butylammonium)tetrabromoplumbate(II), bis(2-phenylethylammonium)tetrachloroplumbate(II), bis(2-phenylethylammonium)-tetrabromoplumbate(II), bis(2-phenylethylammonium)tetraiodoplumbate(II), bis[(4-chlorophenyl)methylammonium]tetrachloromanganate(II), bis[(4-fluorophenyl)methylammonium]tetrachloromanganate(II), and bis(phenylmethylammonium)tetrachloromanganate(II), the crystal structures of which have been measured by X-ray diffraction and deposited in the Cambridge Crystallographic Data Centre.[57] Crystals of the above perovskites were obtained from aqueous solutions using a slow-cooling crystallization method (Fig. S1 and S2, ESI†), where $(C_6H_5\text{–}CH_2\text{–}NH_3)_2MnCl_4$ and $(4\text{-}Cl\text{–}C_6H_4\text{–}CH_2\text{–}NH_3)_2MnCl_4$ crystalized in the monoclinic space group *Cc*, while $(4\text{-}F\text{–}C_6H_4\text{–}CH_2\text{–}NH_3)_2MnCl_4$ crystalized in the orthorhombic space group *Pnma* (Fig. S3, ESI†). Through an antisolvent-induced microprecipitation process facilitated by high-speed stirring and organic surfactants, nanocrystals of metal halide perovskites were synthesized,[58] which were collected and purified by ultracentrifugation, stabilized by surfactants, and finally dispersed in anhydrous chlorobenzene to form stable colloidal suspensions with concentrations of about 200 mg mL^{-1}. As revealed by scanning electron microscopy (SEM) and atomic force microscopy (AFM), nanocrystals prepared from manganese(II)–chloride, lead(II)–chloride, and lead(II)–bromide perovskites exhibited two-dimensional geometry with square, rectangle, or hexagonal shapes as well as widths ranging from hundreds of nanometers to several micrometers, while nanocrystals of $(C_6H_5\text{–}CH_2\text{–}CH_2\text{–}NH_3)_2PbI_4$ appeared as three-dimensional thick cuboids (Fig. S4 and S5, ESI†). A typical batch of $(C_6H_5\text{–}CH_2\text{–}CH_2\text{–}NH_3)_2PbBr_4$ nanoplatelets showed diameters of 400–2000 nm and thicknesses of about 20–40 nm (Fig. 2A, B and Fig. S6, ESI†), corresponding to aspect ratios of 10 to 100. Powder X-ray diffraction (PXRD) analysis of solid films obtained by drying the colloidal dispersions gave diffraction patterns comparable to those calculated from the corresponding single-crystal structures (Fig. 2C and Fig. S7, ESI†), confirming the preservation of perovskite crystal lattices in the nanoplatelets.

Liquid crystalline microstructures in colloidal dispersions of perovskite nanoplatelets

When observed by polarized optical microscopy (POM) between two perpendicularly oriented linear polarizers, the as-prepared colloidal dispersions of metal halide perovskites (except for $(C_6H_5\text{–}CH_2\text{–}CH_2\text{–}NH_3)_2PbI_4$ dispersions, which did not exhibit lyotropic liquid crystallinity) showed birefringent microstructures resembling the discotic nematic liquid crystalline textures formed by other polydispersed nanoparticles with two-dimensional geometry (Fig. 2D).[59,60] Orientations of the local nematic directors could be revealed by inserting a 530-nm full-wavelength retardation plate. A blue hue appears where the

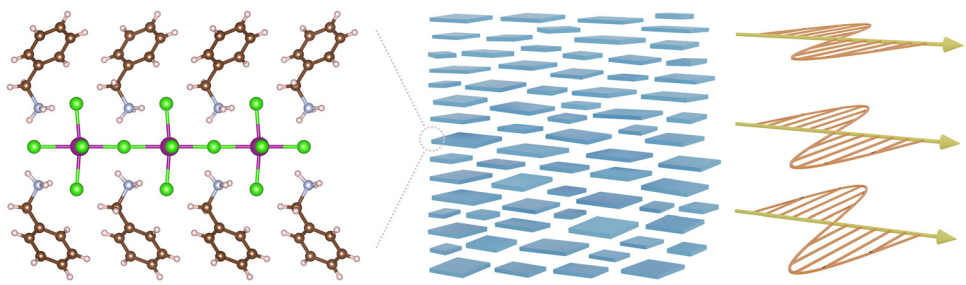

Fig. 1 Schematic diagram illustrating the composition, self-assembled superstructures, and polarized photoluminescence features of perovskite liquid crystals.

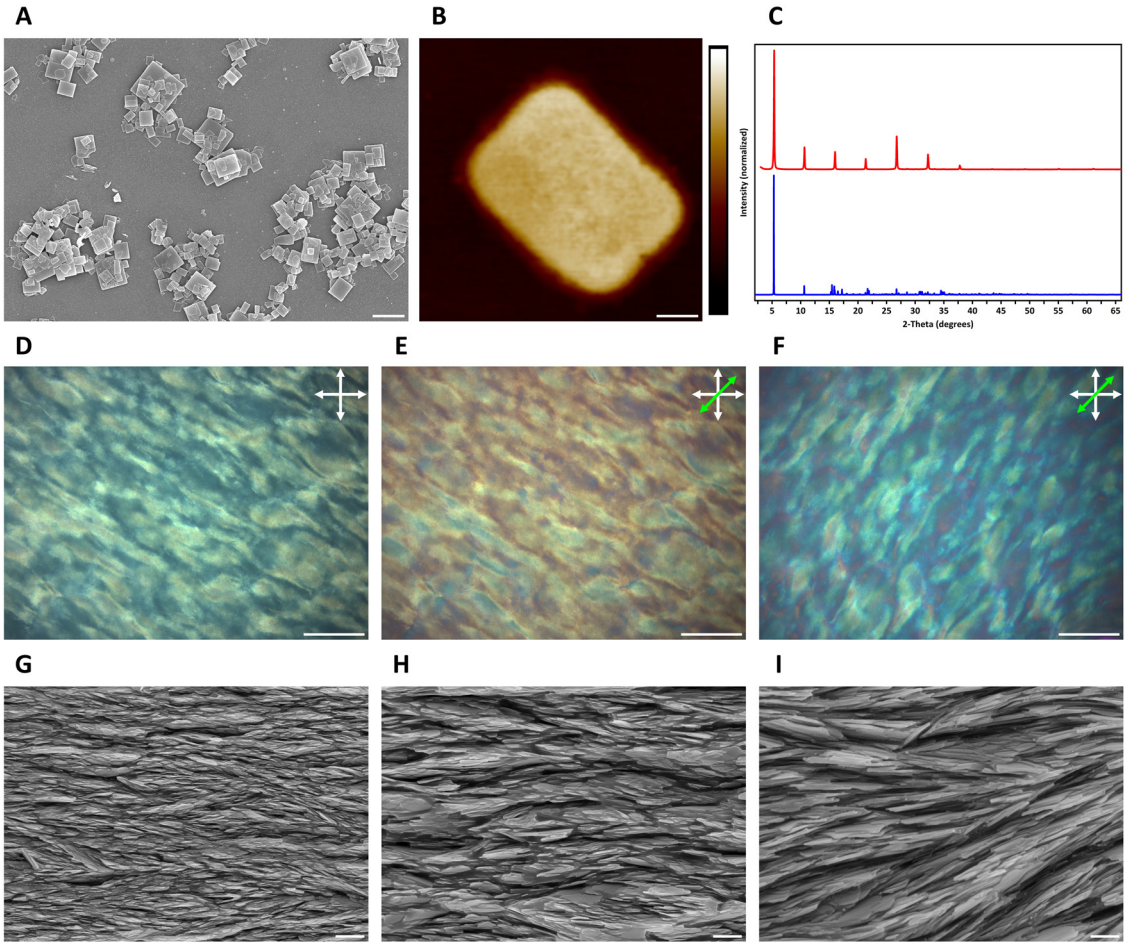

Fig. 2 (A) and (B) SEM (A) and AFM (B) images of $(C_6H_5–CH_2–CH_2–NH_3)_2PbBr_4$ nanoplatelets. (C) PXRD patterns measured from synthesized $(C_6H_5–CH_2–CH_2–NH_3)_2PbBr_4$ nanoplatelets (upper red curve) and simulated based on the single-crystal structure of $(C_6H_5–CH_2–CH_2–NH_3)_2PbBr_4$ (lower blue curve). (D)–(F) POM images showing liquid crystalline textures in a chlorobenzene suspension of $(C_6H_5–CH_2–CH_2–NH_3)_2PbBr_4$ nanoplatelets. The sample was placed between crossed linear polarizers (one in the east–west direction and the other in the north–south direction). Orientations of local nematic directors could be identified by inserting a 530-nm full-wavelength retardation plate with its slow axis oriented in the northeast–southwest direction (E) and (F). The sample was rotated by 90 degrees from (E) to (F). (G)–(I) Cross-sectional SEM images showing the ordered alignment of $(C_6H_5–CH_2–CH_2–NH_3)_2PbBr_4$ nanoplatelets captured within a crosslinked poly(methyl-methacrylate-*co*-styrene) matrix by photo-initiated *in situ* radical polymerization. Color bar: (B) 0–44.6 nm. Scale bars: (A) 2 μm, (B) 100 nm, (D)–(F) 200 μm, (G) 2 μm, (H) 1 μm, (I) 500 nm.

slow axis (with a higher refractive index) of the sample is parallel to the slow axis of the wave plate, while a yellow color would be observed where the fast axis (with a lower refractive index) of the sample is parallel to the slow axis of the wave plate (Fig. 2E, F and Fig. S8, S9, ESI†). Phase behaviors of these colloidal liquid crystals might be explained by the Onsager theory.[61] The critical volume fraction for isotropic-anisotropic phase transitions increases as the average diameter-to-thickness ratio of mesogenic nanoplatelets decreases.[62–66] Since the aspect ratios of cuboidal-shaped $(C_6H_5–CH_2–CH_2–NH_3)_2PbI_4$ nanocrystals were relatively low (1.5–4.0 according to SEM images), the critical volume fraction would be so high that self-assembly may not occur before aggregation happened.

Furthermore, to directly visualize the self-assembly behaviors of perovskite nanoplatelets, the solvent of a liquid crystalline dispersion (1.1 mL) was replaced with a homogeneous mixture of methyl methacrylate (0.6 mL), phenylethylene (styrene, 0.4 mL), divinylbenzene (0.1 mL, cross-linker), and diphenyl(2,4,6-trimethylbenzoyl)phosphine oxide (10 mg, photo-initiator). Microstructures formed in this colloidal suspension could be rapidly captured and solidified within cross-linked poly(methyl-methacrylate-*co*-styrene) networks by photo-initiated *in situ* radical polymerization upon ultraviolet irradiation (365 nm). The resultant perovskite/polymer composite films were cracked to give fresh cross-sections. As revealed by scanning electron microscopy, perovskite nanoplatelets unidirectionally self-assembled into discotic nematic liquid crystalline phases with tangential (*i.e.*, planar) anchoring conditions (Fig. 2G, H and Fig. S10, ESI†), where the nanoplatelets preferentially aligned parallel to the liquid/solid interface at the bottom of the dispersion. At higher magnifications, individual mesogenic nanoplatelets were directly observed with nanometer-scale resolution, which arranged in a face-to-face configuration that could efficiently occupy the space and minimize the excluded volume of this colloidal system (Fig. 2I).[67,68] The structural orderliness of perovskite liquid crystals was also

characterized by X-ray techniques. In the two-dimensional grazing-incidence wide-angle and small-angle X-ray scattering (GIWAXS/GISAXS) patterns of a $(C_6H_5–CH_2–CH_2–NH_3)_2PbBr_4$ liquid crystal placed on a horizontal substrate, the intensities of the diffraction rings concentrated in vertically spaced arcs centered on the meridional axis (Fig. 3A and B), suggesting that the mesogenic nanoplatelets were orderly arranged perpendicular to the vertical direction.[69]

Tunable photoluminescence properties of perovskite liquid crystals

Under ultraviolet irradiation (365 nm), lyotropic liquid crystals of $(C_6H_5–CH_2–CH_2–NH_3)_2PbCl_4$, $(C_6H_5–CH_2–CH_2–NH_3)_2PbBr_4$, and $(CH_3–CH_2–CH_2–CH_2–NH_3)_2PbBr_4$ nanoplatelets exhibited blue- to violet-colored photoluminescence with emission peaks at 510 nm, 415 nm, and 418 nm, as well as quantum yields of 0.56%, 2.92%, and 2.95%, respectively (Fig. 4A–E and Fig. S11, ESI†). Since metal halide perovskites consist of ionic species, the semiconducting properties of perovskite liquid crystals could be readily controlled by compositional adjustments. Liquid crystals of $(C_6H_5–CH_2–CH_2–NH_3)_2PbCl_2Br_2$ showed broad-band white light emissions (with a quantum yield of 1.93%) that may arise from self-trapped excitons (Fig. 4A and Fig. S12, ESI†).[70–72] The emission peaks of $(C_6H_5–CH_2–CH_2–NH_3)_2PbBr_xI_{4-x}$ liquid crystals red-shifted from 415 nm to 509 nm as the value of x decreased from 4 to 1 (liquid crystallinity disappeared when the ratio between bromide and iodide anions was lower than 1/3, which might be caused by the decrease of diameter-to-thickness ratios of perovskite nanoparticles), and in this way liquid crystals with cyan and green photoluminescence were obtained (Fig. 4B, E and Fig. S13, S14, ESI†). The quantum yields of the $(C_6H_5–CH_2–CH_2–NH_3)_2PbBr_2I_2$ and $(C_6H_5–CH_2–CH_2–NH_3)_2PbBrI_3$ liquid crystals were measured to be 0.58% and 0.45%, respectively, where the radiative recombination efficiency in these mixed-halide perovskites may have been reduced by halide segregation, phase separation, and higher concentrations of defects.[73] The defective and inhomogeneous features of doped perovskites also affected the shapes of the photoluminescence emission spectra of $(C_6H_5–CH_2–CH_2–NH_3)_2PbBr_xI_{4-x}$ liquid crystals, resulting in the breaking of symmetry and broadening of the emission peaks (Fig. 4E).

By doping colloidal mesogens of lead bromide perovskites with manganese(II) cations, red-light-emitting liquid crystals of $(C_6H_5–CH_2–CH_2–NH_3)_2Pb_{0.8}Mn_{0.2}Br_4$ were prepared (Fig. 4C, D and Fig. S15, ESI†). Moreover, liquid crystalline dispersions of $(C_6H_5–CH_2–CH_2–NH_3)_2PbBr_xI_{4-x}$ nanoplatelets with x = 2.35, 2.20, 2.00, 1.85, and 1.40 showed emission wavelengths of 470 nm, 475 nm, 480 nm, 485 nm, and 490 nm, respectively (Fig. 4F), indicating that the energy band gaps of perovskite liquid crystals could be precisely adjusted over a wide wavelength range in the visible region. Preservation of perovskite crystalline lattices in the above liquid crystals containing mixed divalent metal cations or halide anions was confirmed by powder X-ray diffraction analysis.

Polarized luminescence and light-responsiveness of perovskite liquid crystals

Simultaneously possessing long-range structural anisotropy and semiconducting properties, perovskite liquid crystals might be able to emit and/or detect polarized photons like other luminescent materials with anisotropic structures. A colloidal liquid crystalline dispersion of perovskite nanoplatelets was sandwiched between a pair of two plane-parallel glass plates that were separated by a distance of about 100 micrometers, and this thin flat layer of liquid crystal was illuminated by unpolarized ultraviolet light (365 nm) from the direction perpendicular to it. Photoluminescence emission spectra were measured from the tangential direction of the liquid crystal layer, where a rotatable linear polarizer was placed between the liquid crystal and the spectrometer to examine the polarization anisotropy of the emitted light. While rotating the polarizer, correlations between the polarization angle (*i.e.*, the angle of the polarization plane with reference to the thin liquid

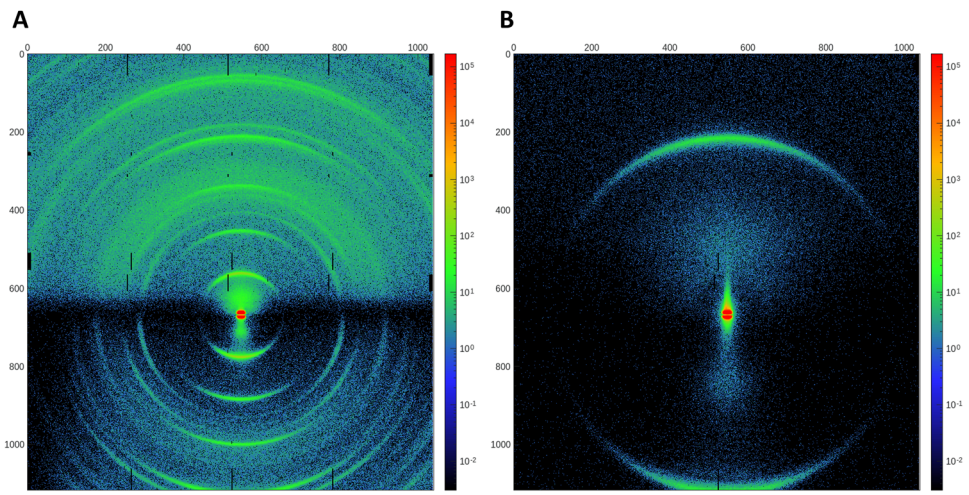

Fig. 3 (A) and (B) Two-dimensional grazing-incidence wide-angle (A) and small-angle (B) X-ray scattering patterns of a $(C_6H_5–CH_2–CH_2–NH_3)_2PbBr_4$ liquid crystal.

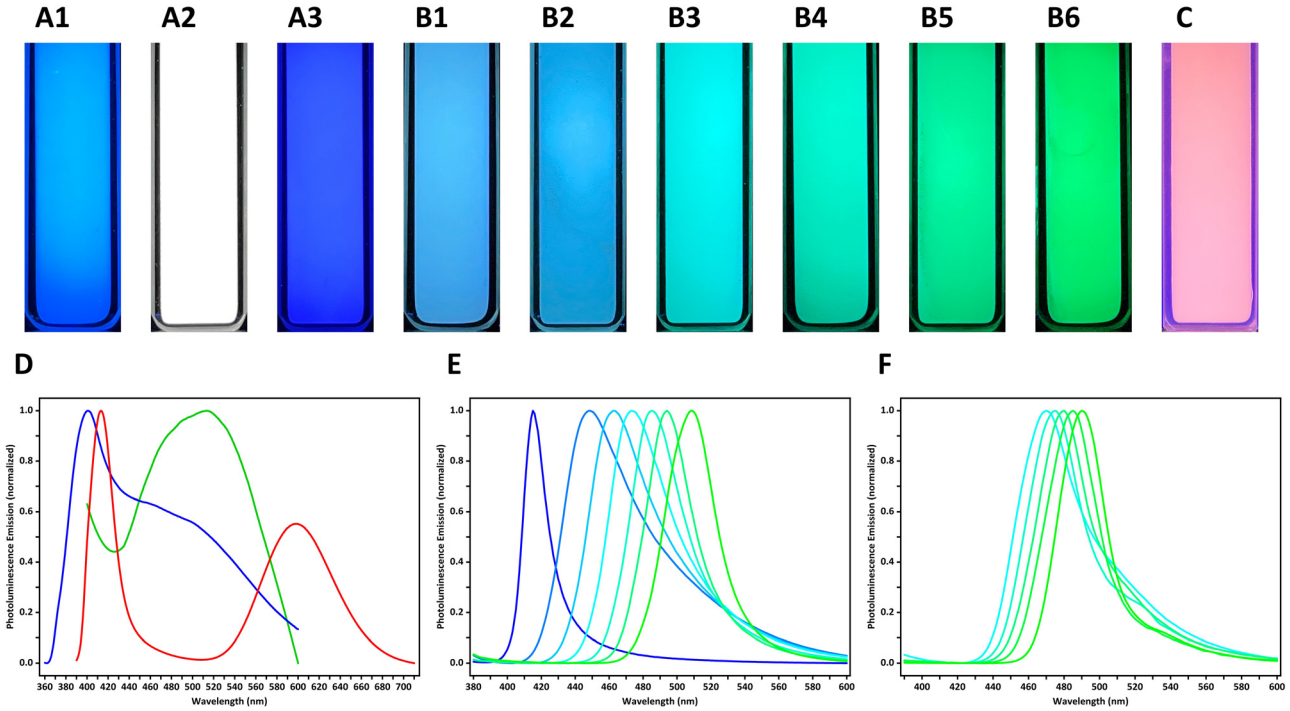

Fig. 4 (A)–(C) Photographs showing the emission of colloidal liquid crystalline dispersions (sealed in quartz cuvettes with an internal width of 10 mm and an optical path length of 0.5 mm) of metal halide perovskites under 365-nm ultraviolet light: PEA_2PbCl_4 (A_1), $PEA_2PbCl_2Br_2$ (A_2), PEA_2PbBr_4 (A_3), $PEA_2PbBr_{3.5}I_{0.5}$ (B_1), $PEA_2PbBr_3I_1$ (B_2), $PEA_2PbBr_{2.5}I_{1.5}$ (B_3), $PEA_2PbBr_2I_2$ (B_4), $PEA_2PbBr_{1.5}I_{2.5}$ (B_5), $PEA_2PbBr_1I_3$ (B_6), and $PEA_2Pb_{0.8}Mn_{0.2}Br_4$ (C), where PEA represents 2-phenylethylammonium cations ($C_6H_5–CH_2–CH_2–NH_3^+$). (D)–(F) Photoluminescence spectra of liquid crystals of different perovskites (excited by 365-nm light): (D) PEA_2PbCl_4 (green), $PEA_2PbCl_2Br_2$ (blue), and $PEA_2Pb_{0.8}Mn_{0.2}Br_4$ (red); (E) $PEA_2PbBr_xI_{4-x}$, where x = 4.0, 3.5, 3.0, 2.5, 2.0, 1.5, and 1.0 from left to right; (F) $PEA_2PbBr_xI_{4-x}$, where x = 2.35, 2.20, 2.00, 1.85, and 1.40 from left to right.

crystalline layer) and the integrated photoluminescence intensity after passing through the polarizer were recorded. In a typical experiment, the visible light emitted by a colloidal liquid crystal of $(C_6H_5–CH_2–CH_2–NH_3)_2PbBr_4$ was found to be linearly polarized along the direction parallel to the mesogenic nanoplatelets (*i.e.*, parallel to the glass substrates due to planar anchoring), and a degree of polarization (defined as DOP = $(I_{max} - I_{min})/(I_{max} + I_{min})$, where I_{max} and I_{min} are the maximum and minimum emission intensities, respectively) of about 0.14 was revealed (Fig. 5A).

Afterwards, the semiconducting liquid crystal layer was irradiated in the tangential direction with polarized ultraviolet light (365 nm), and its photoluminescence spectrum was collected from the normal direction. A representative sample of $(C_6H_5–CH_2–CH_2–NH_3)_2PbBr_4$ liquid crystals exhibited polarization-dependent photo-responsiveness as its emission intensity reached maximum values when the incident excitation light was linearly polarized parallel to the perovskite nanoplatelets, and the degree of polarization was measured to be about 0.19 (Fig. 5B). Colloidal liquid crystalline dispersions of $(C_6H_5–CH_2–CH_2–NH_3)_2PbCl_4$, $(C_6H_5–CH_2–CH_2–NH_3)_2PbCl_2Br_2$, $(C_6H_5–CH_2–CH_2–NH_3)_2PbBr_2I_2$, and $(C_6H_5–CH_2–CH_2–NH_3)_2PbBrI_3$ nanoplatelets also showed anisotropic light-emitting properties as well as responsiveness to polarized photons, with degrees of polarization ranging from 0.06 to 0.32 as determined using similar experimental protocols (Fig. S16 and Table S1, ESI†). Further improvements in the degrees of polarization might be achieved by increasing the structural orderliness of the liquid crystalline dispersion, or by removing perovskite nanocrystals with low aspect ratios since these colloidal components would emit non-polarized light upon excitation and therefore decrease the overall DOP of the liquid crystal layer.[74,75] Moreover, by spin-coating perovskite liquid crystals onto interdigitated electrodes (indium tin oxide on transparent glass substrates; each device consisted of 16 pairs of digits that were 13 mm long and 0.2 mm wide, and every two adjacent digits were separated by a distance of 0.2 mm), electrical and photoelectronic properties of dried liquid crystalline films could be preliminarily evaluated. The conductivities of the films remarkably increased as the power density of incident ultraviolet light was raised from 0 to 35.30 milliwatts per centimeter squared (Fig. 5C), indicating that charge-carriers were generated when photons struck the semiconducting mesogenic nanoplatelets. Under pulsed illumination, the films produced photocurrents with abrupt and reproducible on–off switching characteristics (Fig. 5D), the rise and decay times (10–90%) of which were measured to be approximately 20 milliseconds (Fig. 5E). Photocurrents in perovskite liquid crystalline films were also investigated with respect to the polarization angle of the excitation light (365 nm, 35.30 mW cm^{-2} before passing through the linear polarizer), where maximum responsiveness occurred when the polarization plane of the incident light was parallel to the plate-shaped mesogens (Fig. 5F). Although it was difficult to

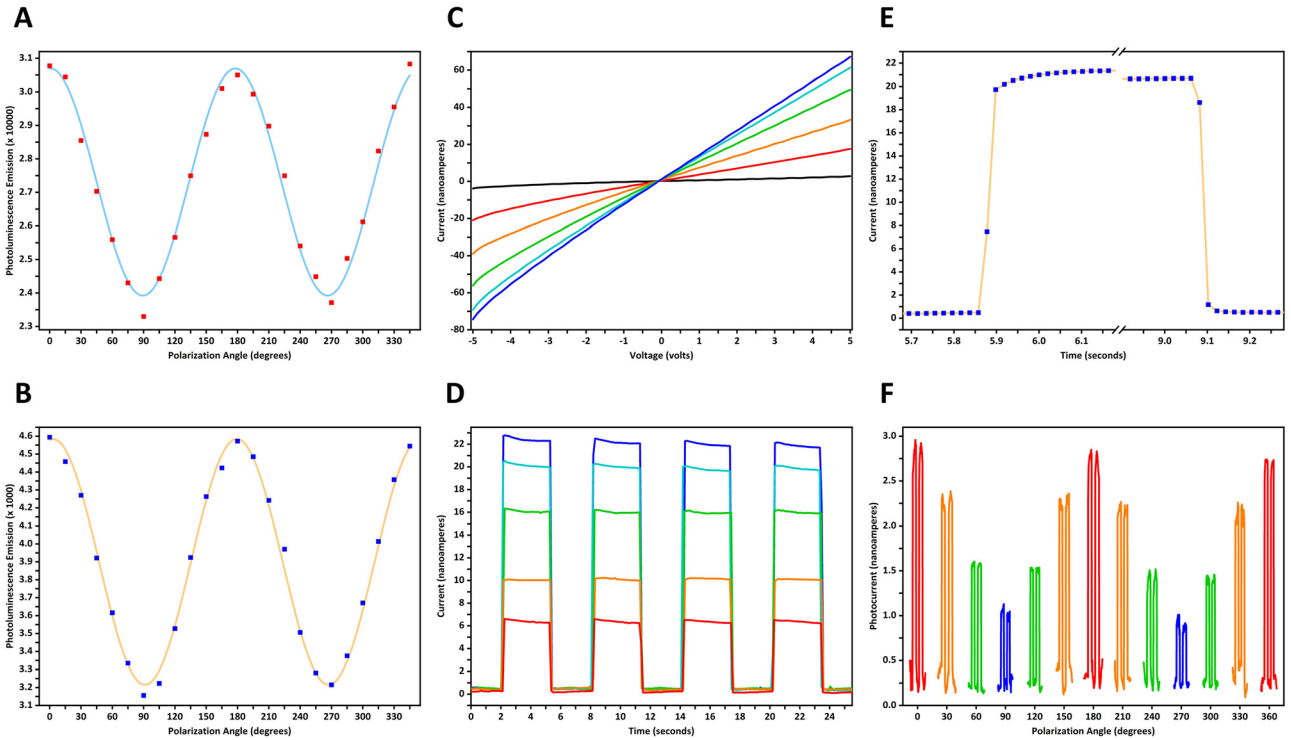

Fig. 5 (A) and (B) The integrated photoluminescence intensity of a $(C_6H_5–CH_2–CH_2–NH_3)_2PbBr_4$ liquid crystal as a function of the polarization angle of the emission light (A) or the excitation light (B). Sine-squared waveforms (plotted as solid curves) have been fitted to the experimental results (square symbols). (C) and (D) Current–voltage characteristics (C) and time-resolved photocurrents (D) of a $(C_6H_5–CH_2–CH_2–NH_3)_2PbBr_4$ liquid crystalline film under 365-nm illumination with power densities of 0 (black), 3.57 (red), 8.15 (orange), 17.65 (green), 27.20 (cyan), and 35.30 mW cm^{-2} (blue). (E) Rise and decay kinetics of the photocurrent during an on–off cycle of light (365 nm, 35.30 mW cm^{-2}). (F) Photocurrents of a $(C_6H_5–CH_2–CH_2–NH_3)_2PbBr_4$ liquid crystalline film in relation to the polarization angle of the incident light. A constant bias voltage of 1.5 volts was applied in (D)–(F).

quantitatively determine the contributions of anisotropic absorption of polarized light in thin films with discotic nematic ordering to the above experimental results,[76] the overall performances of perovskite liquid crystals suggest that these soft and ordered semiconductors may find applications in the generation and/or detection of polarized photons.

Conclusion

In summary, lyotropic liquid crystalline dispersions formed by plate-shaped colloidal nanocrystals of two-dimensional organic–inorganic metal halide perovskites were prepared through antisolvent-induced micro-precipitation processes, where the perovskites may consist of divalent manganese(II) or lead(II) cations, different types of aromatic or aliphatic ammonium spacers, and halide anions such as chloride, bromide, iodide, or their mixtures. Liquid crystals of lead halide perovskites exhibited linearly polarized photoluminescence and polarization-dependent responses to incident photons, and the semiconducting band gaps of these anisotropic fluids could be precisely adjusted over a relatively wide range by compositional variations, giving rise to a series of luminescent liquid crystals with emission wavelengths tunable from blue to green at intervals of 5 nm. These results suggest that transforming metal halide perovskites into colloidal liquid crystalline mesogens might be a promising approach to the systematic development of semiconducting materials with structural orderliness and readily controllable band gaps, which may find applications in polarized light sources, digital displays, and optical communication systems.

Experimental methods

Synthesis of metal halide perovskites

In a representative experiment, a clear and hot (heated to 373 K) aqueous solution containing hydrochloric acid (11.9 mol L^{-1}), manganese(II) acetate tetrahydrate (0.10 mol L^{-1}), and [(4-fluorophenyl)methyl]amine (0.20 mol L^{-1}) was slowly cooled to 298 K over a period of 2 hours in a glass flask without disturbance, giving light pink-colored plate-shaped crystals of $(4\text{-}F\text{-}C_6H_4\text{-}CH_2\text{-}NH_3)_2MnCl_4$. The crystals were collected by vacuum filtration, then washed five times with cyclohexane, and finally thoroughly dried at 298 K under vacuum. Crystals of $(4\text{-}Cl\text{-}C_6H_4\text{-}CH_2\text{-}NH_3)_2MnCl_4$ and $(C_6H_5\text{-}CH_2\text{-}NH_3)_2MnCl_4$ were synthesized with the same experimental parameters using [(4-chlorophenyl)methyl]amine and phenylmethylamine as precursors for organic ammonium cations, respectively.

As revealed by single-crystal X-ray diffraction analysis, $(C_6H_5\text{-}CH_2\text{-}NH_3)_2MnCl_4$ crystalized in the monoclinic space group $C1c1$ with unit cell parameters of a = 3.2430(8) nm, b = 0.51630(14) nm, c = 1.0327(3) nm, alpha = gamma = 90 degrees,

beta = 98.217(7) degrees, and Z = 4; (4-F–C_6H_4–CH_2–NH_3)$_2MnCl_4$ crystalized in the orthorhombic space group *Pnma* with unit cell parameters of a = 1.04140(6) nm, b = 3.2068(2) nm, c = 0.51535(3) nm, alpha = beta = gamma = 90 degrees, and Z = 4; while (4-Cl–C_6H_4–CH_2–NH_3)$_2MnCl_4$ crystalized in the monoclinic space group *Cc* with unit cell parameters of a = 3.4411(4) nm, b = 0.51714(5) nm, c = 1.04163(10) nm, alpha = gamma = 90 degrees, beta = 98.670(4) degrees, and the number of formula units per unit cell Z = 4.

For lead-based perovskites, crystals of (CH_3–CH_2–CH_2–CH_2–NH_3)$_2PbBr_4$ were synthesized using hydrobromic acid (8.8 mol L^{-1}), lead(II) oxide (0.50 mol L^{-1}), and *n*-butylamine (1.00 mol L^{-1}); crystals of (C_6H_5–CH_2–CH_2–NH_3)$_2PbBr_4$ were synthesized using hydrobromic acid (8.8 mol L^{-1}), lead(II) oxide (0.15 mol L^{-1}), and 2-phenylethylamine (0.30 mol L^{-1}); crystals of (C_6H_5–CH_2–CH_2–NH_3)$_2PbCl_4$ were synthesized using hydrochloric acid (11.9 mol L^{-1}), lead(II) oxide (0.15 mol L^{-1}), and 2-phenylethylamine (0.30 mol L^{-1}); while crystals of (C_6H_5–CH_2–CH_2–NH_3)$_2PbI_4$ were synthesized using hydroiodic acid (7.5 mol L^{-1}), lead(II) oxide (0.20 mol L^{-1}), and 2-phenylethylamine (0.40 mol L^{-1}).

Preparation of liquid crystalline dispersions of perovskites

In a typical procedure, a clear *N*,*N*-dimethylformamide solution (0.30 mL; denoted as V1) of (C_6H_5–CH_2–CH_2–NH_3)$_2PbBr_4$ (1.0 mol L^{-1}; C1) crystals was slowly added to an anhydrous chlorobenzene solution (10.0 mL; the chlorobenzene was pre-dried over anhydrous copper(II) sulfate that had been heated at 523 K for 3 hours in a round-bottom glass flask and then cooled to 298 K with the flask sealed with a rubber stopper) of *cis*-9-octadecenoic acid (oleic acid; 1 : 1000 by volume, around 3.151 mmol L^{-1}; C2) and *cis*-1-amino-9-octadecene (oleylamine; 1 : 1000 by volume, around 3.039 mmol L^{-1}; C3) at a stirring speed of 2400 revolutions per minute. About 5 minutes later, the reaction mixture was centrifuged at 9000 rpm for 10 minutes in a sealed centrifuge tube. The supernatant fluid was decanted to remove *N*,*N*-dimethylformamide and excess ions, and the solids of perovskite nanocrystals were redispersed in a chlorobenzene solution (10.0 mL) of *cis*-9-octadecenoic acid (1 : 1000 by volume; C4) and *cis*-1-amino-9-octadecene (1 : 1000 by volume; C5) by sonication. Afterwards, the dispersion was centrifuged again at 9000 rpm for 30 minutes, and the solid sediments were redispersed in a chlorobenzene solution (1.0 mL) of *cis*-9-octadecenoic acid (1 : 1000 by volume; C6) and *cis*-1-amino-9-octadecene (1 : 1000 by volume; C7) by sonication to form a concentrated suspension of perovskite nanocrystals, which exhibited lyotropic liquid crystalline behaviors when examined under polarized optical microscopy.

With some modifications to the above procedure, colloidal liquid crystals of other perovskites could be synthesized. Liquid crystalline dispersions of (C_6H_5–CH_2–NH_3)$_2MnCl_4$, (4-F–C_6H_4–CH_2–NH_3)$_2MnCl_4$, and (4-Cl–C_6H_4–CH_2–NH_3)$_2MnCl_4$ were prepared with V1 = 0.60 mL, C1 = 0.75 mol L^{-1}, C2 = 1 : 2000 by volume (about 1.575 mmol L^{-1}), C3 = 1 : 2000 by volume (about 1.520 mmol L^{-1}), and C4 = C5 = C6 = C7 = 0. Liquid crystals of (CH_3–CH_2–CH_2–CH_2–NH_3)$_2PbBr_4$ were obtained with V1 = 0.10 mL and C1 = 1.5 mol L^{-1}. Liquid crystals of (C_6H_5–CH_2–CH_2–NH_3)$_2PbCl_4$ were prepared with V1 = 0.60 mL and C1 = 0.5 mol L^{-1}.

Liquid crystals of (C_6H_5–CH_2–CH_2–NH_3)$_2PbCl_2Br_2$ were obtained by using an *N*,*N*-dimethylformamide solution (0.30 mL) of (C_6H_5–CH_2–CH_2–NH_3)$_2PbCl_4$ (0.25 mol L^{-1}) and (C_6H_5–CH_2–CH_2–NH_3)$_2PbBr_4$ (0.25 mol L^{-1}) as the perovskite precursor solution. Liquid crystals of (C_6H_5–CH_2–CH_2–NH_3)$_2PbBr_xI_{4-x}$ were prepared with an *N*,*N*-dimethylformamide solution (0.30 mL) of (C_6H_5–CH_2–CH_2–NH_3)$_2PbBr_4$ (x/4 mol L^{-1}) and (C_6H_5–CH_2–CH_2–NH_3)$_2PbI_4$ ($(4-x)$/4 mol L^{-1}) as the perovskite precursor solution. Liquid crystals of (C_6H_5–CH_2–CH_2–NH_3)$_2Pb_{0.8}Mn_{0.2}Br_4$ were prepared by using an *N*,*N*-dimethylformamide solution (0.375 mL) of (C_6H_5–CH_2–CH_2–NH_3)$_2PbBr_4$ (0.8 mol L^{-1}) and $MnBr_2$ (0.2 mol L^{-1}) as the perovskite precursor. All other experimental parameters were kept the same as in the preparation of (C_6H_5–CH_2–CH_2–NH_3)$_2PbBr_4$ liquid crystals.

Data availability

The data supporting this article have been included as part of the ESI.†

Conflicts of interest

The authors declare no conflict of interest.

Acknowledgements

This research was financially supported by the National Natural Science Foundation of China (Young Scientists Fund 22205255), the Youth Innovation Promotion Association of the Chinese Academy of Sciences (2023336), the Natural Science Foundation of Jiangsu Province (Young Scientists Fund BK20220297), the Jiangsu Provincial High-Level Innovation and Entrepreneurship Talents Program (JSSCRC2022463; JSSCBS20211429), the Gusu Innovation and Entrepreneurship Leading Talents Program (ZXL2022467), and the Suzhou Institute of Nano-Tech and Nano-Bionics (E1551302; E2551306; E43E1304).

References

1 S. H. Chen, D. Katsis, A. W. Schmid, J. C. Mastrangelo, T. Tsutsui and T. N. Blanton, *Nature*, 1999, **397**, 506–508.
2 M. O'Neill and S. M. Kelly, *Adv. Mater.*, 2003, **15**, 1135–1146.
3 Y. Wang, J. Shi, J. Chen, W. Zhu and E. Baranoff, *J. Mater. Chem. C*, 2015, **3**, 7993–8005.
4 G. Singh, M. Fisch and S. Kumar, *Rep. Prog. Phys.*, 2016, **79**, 056502.
5 Y. Shi, J. Han, X. Jin, W. Miao, Y. Zhang and P. Duan, *Adv. Sci.*, 2022, **9**, 2201565.
6 Y. Wu, M. Li, Z. Zheng, Z.-Q. Yu and W.-H. Zhu, *J. Am. Chem. Soc.*, 2023, **145**, 12951–12966.
7 S. Huang, Q. Wu, R. Luo, B. Tan, Y. Yuan and H. Zhang, *Macromolecules*, 2024, **57**, 9017–9029.

8 C. Zhang, K. Nakano, M. Nakamura, F. Araoka, K. Tajima and D. Miyajima, *J. Am. Chem. Soc.*, 2020, **142**, 3326–3330.
9 Y. Wang, D. Fang, T. Fu, M. U. Ali, Y. Shi, Y. He, Z. Hu, C. Yan, Z. Mei and H. Meng, *Mater. Chem. Front.*, 2020, **4**, 3546–3555.
10 H. Coles and S. Morris, *Nat. Photonics*, 2010, **4**, 676–685.
11 L.-J. Chen, J.-H. Dai, J.-D. Lin, T.-S. Mo, H.-P. Lin, H.-C. Yeh, Y.-C. Chuang, S.-A. Jiang and C.-R. Lee, *ACS Appl. Mater. Interfaces*, 2018, **10**, 33307–33315.
12 I. O. Shklyarevskiy, P. Jonkheijm, N. Stutzmann, D. Wasserberg, H. J. Wondergem, P. C. M. Christianen, A. P. H. J. Schenning, D. M. de Leeuw, Ž. Tomović, J. Wu, K. Müllen and J. C. Maan, *J. Am. Chem. Soc.*, 2005, **127**, 16233–16237.
13 A. J. J. M. van Breemen, P. T. Herwig, C. H. T. Chlon, J. Sweelssen, H. F. M. Schoo, S. Setayesh, W. M. Hardeman, C. A. Martin, D. M. de Leeuw, J. J. P. Valeton, C. W. M. Bastiaansen, D. J. Broer, A. R. Popa-Merticaru and S. C. J. Meskers, *J. Am. Chem. Soc.*, 2018, **128**, 2336–2345.
14 M. J. Han, D. Wei, Y. H. Kim, H. Ahn, T. J. Shin, N. A. Clark, D. M. Walba and D. K. Yoon, *ACS Cent. Sci.*, 2018, **4**, 1495–1502.
15 Y. Sagara and T. Kato, *Angew. Chem., Int. Ed.*, 2008, **47**, 5175–5178.
16 X. Zhang, L. Li, Y. Chen, C. Valenzuela, Y. Liu, Y. Yang, Y. Feng, L. Wang and W. Feng, *Angew. Chem., Int. Ed.*, 2024, **63**, e202404202.
17 S. Sergeyev, W. Pisula and Y. H. Geerts, *Chem. Soc. Rev.*, 2007, **36**, 1902–1929.
18 W. Pisula, M. Zorn, J. Y. Chang, K. Müllen and R. Zentel, *Macromol. Rapid Commun.*, 2009, **30**, 1179–1202.
19 K. Binnemans, *J. Mater. Chem.*, 2009, **19**, 448–453.
20 T. Kato, M. Yoshio, T. Ichikawa, B. Soberats, H. Ohno and M. Funahashi, *Nat. Rev. Mater.*, 2017, **2**, 17001.
21 L. Chen, C. Chen, Y. Sun, S. Lu, H. Huo, T. Tan, A. Li, X. Li, G. Ungar, F. Liu and M. Zhang, *Angew. Chem., Int. Ed.*, 2020, **59**, 10143–10150.
22 X. Hao, B. Xiong, M. Ni, B. Tang, Y. Ma, H. Peng, X. Zhou, I. I. Smalyukh and X. Xie, *ACS Appl. Mater. Interfaces*, 2020, **12**, 53058–53066.
23 Y. Wu, M. Li, Z. Zheng, Z.-Q. Yu and W.-H. Zhu, *J. Am. Chem. Soc.*, 2023, **145**, 12951–12966.
24 L. Li, J. Walda, L. Manna and A. P. Alivisatos, *Nano Lett.*, 2002, **2**, 557–560.
25 J. E. Kim, T. H. Han, S. H. Lee, J. Y. Kim, C. W. Ahn, J. M. Yun and S. O. Kim, *Angew. Chem., Int. Ed.*, 2011, **50**, 3043–3047.
26 Z. Xu and C. Gao, *ACS Nano*, 2011, **5**, 2908–2915.
27 S. Zhang, C. I. Pelligra, G. Keskar, P. W. Majewski, F. Ren, L. D. Pfefferle and C. O. Osuji, *ACS Nano*, 2011, **5**, 8357–8364.
28 N. Miyamoto, S. Yamamoto, K. Shimasaki, K. Harada and Y. Yamauchi, *Chem. – Asian J.*, 2011, **6**, 2936–2939.
29 J. Hou, Y. Zheng, Y. Su, W. Zhang, T. Hoshide, F. Xia, J. Jie, Q. Li, Z. Zhao, R. Ma, T. Sasaki and F. Geng, *J. Am. Chem. Soc.*, 2015, **137**, 13200–13208.
30 R. Jalili, S. Aminorroaya-Yamini, T. M. Benedetti, S. H. Aboutalebi, Y. Chao, G. G. Wallace and D. L. Officer, *Nanoscale*, 2016, **8**, 16862–16867.
31 T. Hoshide, Y. Zheng, J. Hou, Z. Wang, Q. Li, Z. Zhao, R. Ma, T. Sasaki and F. Geng, *Nano Lett.*, 2017, **17**, 3543–3549.
32 Y. Xia, T. S. Mathis, M.-Q. Zhao, B. Anasori, A. Dang, Z. Zhou, H. Cho, Y. Gogotsi and S. Yang, *Nature*, 2018, **557**, 409–412.
33 B. T. Hogan, E. Kovalska, M. O. Zhukova, M. Yildirim, A. Baranov, M. F. Craciun and A. Baldycheva, *Nanoscale*, 2019, **11**, 16886–16895.
34 Y. Wang, Y. Zheng, L. Sheng, J. Zhao and Y. Li, *Nanoscale*, 2020, **12**, 1374–1383.
35 X. Yang, X. Jin, T. Zhao and P. Duan, *Mater. Chem. Front.*, 2021, **5**, 4821–4832.
36 Q. A. Akkerman, S. G. Motti, A. R. Srimath Kandada, E. Mosconi, V. D'Innocenzo, G. Bertoni, S. Marras, B. A. Kamino, L. Miranda, F. De Angelis, A. Petrozza, M. Prato and L. Manna, *J. Am. Chem. Soc.*, 2016, **138**, 1010–1016.
37 S. Sun, D. Yuan, Y. Xu, A. Wang and Z. Deng, *ACS Nano*, 2016, **10**, 3648–3657.
38 M. C. Weidman, M. Seitz, S. D. Stranks and W. A. Tisdale, *ACS Nano*, 2016, **10**, 7830–7839.
39 M. D. Smith, B. A. Connor and H. I. Karunadasa, *Chem. Rev.*, 2019, **119**, 3104–3139.
40 J. Yuan, A. Hazarika, Q. Zhao, X. Ling, T. Moot, W. Ma and J. M. Luther, *Joule*, 2020, **4**, 1160–1185.
41 B. J. Bohn, Y. Tong, M. Gramlich, M. L. Lai, M. Döblinger, K. Wang, R. L. Z. Hoye, P. Müller-Buschbaum, S. D. Stranks, A. S. Urban, L. Polavarapu and J. Feldmann, *Nano Lett.*, 2018, **18**, 5231–5238.
42 Y. Wei, Y. Xu, Q. Wang, J. Wang, H. Lu and J. Zhu, *Chem. Commun.*, 2020, **56**, 5413–5416.
43 J. Cui, Y. Liu, Y. Deng, C. Lin, Z. Fang, C. Xiang, P. Bai, K. Du, X. Zuo, K. Wen, S. Gong, H. He, Z. Ye, Y. Gao, H. Tian, B. Zhao, J. Wang and Y. Jin, *Sci. Adv.*, 2021, **7**, eabg8458.
44 Q. Zhang, R. Su, X. Liu, J. Xing, T. C. Sum and Q. Xiong, *Adv. Funct. Mater.*, 2016, **26**, 6238–6245.
45 J. Sun, J. Wu, X. Tong, F. Lin, Y. Wang and Z. M. Wang, *Adv. Sci.*, 2018, **5**, 1700780.
46 K. Wang, C. Wu, D. Yang, Y. Jiang and S. Priya, *ACS Nano*, 2018, **12**, 4919–4929.
47 Y. Wang, X. Liu, Q. He, G. Chen, D. Xu, X. Chen, W. Zhao, J. Bao, X. Xu, J. Liu and X. Wang, *Adv. Funct. Mater.*, 2021, **31**, 2011251.
48 Y.-M. You, W.-Q. Liao, D. Zhao, H.-Y. Ye, Y. Zhang, Q. Zhou, X. Niu, J. Wang, P.-F. Li, D.-W. Fu, Z. Wang, S. Gao, K. Yang, J.-M. Liu, J. Li, Y. Yan and R.-G. Xiong, *Science*, 2017, **357**, 306–309.
49 L. Li, X. Liu, Y. Li, Z. Xu, Z. Wu, S. Han, K. Tao, M. Hong, J. Luo and Z. Sun, *J. Am. Chem. Soc.*, 2019, **141**, 2623–2629.
50 M. Sun, C. Zheng, Y. Gao, A. Johnston, A. M. Najarian, P. Wang, O. Voznyy, S. Hoogland and E. H. Sargent, *Adv. Mater.*, 2021, **33**, 2006368.
51 S. Bera, S. Shyamal and N. Pradhan, *J. Am. Chem. Soc.*, 2021, **143**, 14895–14906.

52 X. Xia, J. Peng, Q. Wan, X. Wang, Z. Fan, J. Zhao and F. Li, *ACS Appl. Mater. Interfaces*, 2021, **13**, 17677–17689.
53 D. Devadiga, A. Tantri Nagaraja, D. Devadiga and M. Selvakumar, *Energy Fuels*, 2024, **38**, 854–868.
54 Y. Yang, C. Liu, Y. Ding, B. Ding, J. Xu, A. Liu, J. Yu, L. Grater, H. Zhu, S. S. Hadke, V. K. Sangwan, A. S. R. Bati, X. Hu, J. Li, S. M. Park, M. C. Hersam, B. Chen, M. K. Nazeeruddin, M. G. Kanatzidis and E. H. Sargent, *Nat. Energy*, 2024, **9**, 316–323.
55 J.-H. Im, M. Han, J. Hong, H. Kim, K.-S. Oh, T. Choi, A. R. bin, M. Yusoff, M. Vasilopoulou, E. Lee, C.-C. Hwang, Y.-Y. Noh and Y.-K. Kim, *ACS Nano*, 2025, **19**, 1177–1189.
56 A. Stergiou, L. Leccioli, D. Ricci, M. L. Zaffalon, S. Brovelli, F. B. Bombelli, G. Terraneo, P. Metrangolo and G. Cavallo, *Angew. Chem., Int. Ed.*, 2024, **63**, e202408570.
57 CCDC deposition numbers for the perovskite crystal structures involved in this research: $(C_6H_5–CH_2–NH_3)_2MnCl_4$ (2131311), $(4\text{-}F–C_6H_4–CH_2–NH_3)_2MnCl_4$ (2040553), $(4\text{-}Cl–C_6H_4–CH_2–NH_3)_2MnCl_4$ (2047191), $(C_6H_5–CH_2–CH_2–NH_3)_2PbCl_4$ (1209430), $(C_6H_5–CH_2–CH_2–NH_3)_2PbBr_4$ (1209433), $(C_6H_5–CH_2–CH_2–NH_3)_2PbI_4$ (1542461), $(CH_3–CH_2–CH_2–CH_2–NH_3)_2PbBr_4$ (1521054).
58 P.-X. Wang, *Chem. Commun.*, 2021, **57**, 5051–5054.
59 M. C. D. Mourad, E. J. Devid, M. M. van Schooneveld, C. Vonk and H. N. W. Lekkerkerker, *J. Phys. Chem. B*, 2008, **112**, 10142–10152.
60 P. Davidson, C. Penisson, D. Constantin and J.-C. P. Gabriel, *Proc. Natl. Acad. Sci. U. S. A.*, 2018, **115**, 6662–6667.
61 L. Onsager, *Ann. Acad. Sci.*, 1949, **51**, 627–659.
62 P. A. Forsyth, S. Marčelja, D. J. Mitchell and B. W. Ninham, *J. Chem. Soc., Faraday Trans. 2*, 1977, **73**, 84–88.
63 J. D. Parsons, *Phys. Rev. A*, 1979, **19**, 1225–1230.
64 A. Mourchid, A. Delville, J. Lambard, E. LeColier and P. Levitz, *Langmuir*, 1995, **11**, 1942–1950.
65 L. Harnau, D. Rowan and J.-P. Hansen, *J. Chem. Phys.*, 2002, **117**, 11359–11365.
66 H. H. Wensink and H. N. W. Lekkerkerker, *Mol. Phys.*, 2009, **107**, 2111–2118.
67 F. M. van der Kooij, K. Kassapidou and H. N. W. Lekkerkerker, *Nature*, 2000, **406**, 868–871.
68 H. N. W. Lekkerkerker and G. J. Vroege, *Philos. Trans. R. Soc., A*, 2013, **371**, 20120263.
69 E. van den Pol, A. Lupascu, M. A. Diaconeasa, A. V. Petukhov, D. V. Byelov and G. J. Vroege, *J. Phys. Chem. Lett.*, 2010, **1**, 2174–2178.
70 S. Yang, Z. Lin, J. Wang, Y. Chen, Z. Liu, E. Yang, J. Zhang and Q. Ling, *ACS Appl. Mater. Interfaces*, 2018, **10**, 15980–15987.
71 J. Luo, X. Wang, S. Li, J. Liu, Y. Guo, G. Niu, L. Yao, Y. Fu, L. Gao, Q. Dong, C. Zhao, M. Leng, F. Ma, W. Liang, L. Wang, S. Jin, J. Han, L. Zhang, J. Etheridge, J. Wang, Y. Yan, E. H. Sargent and J. Tang, *Nature*, 2018, **563**, 541–545.
72 M. D. Smith and H. I. Karunadasa, *Acc. Chem. Res.*, 2018, **51**, 619–627.
73 A. J. Knight and L. M. Herz, *Energy Environ. Sci.*, 2020, **13**, 2024–2046.
74 J. Sha, H. Lu, M. Zhou, G. Xia, Y. Fang, G. Zhang, L. Qiu, J. Yang and Y. Ding, *Org. Electron.*, 2017, **50**, 177–183.
75 W. Gong, G. Huang, M. Zhou, C. Fan, Y. Yuan and H. Zhang, *ACS Appl. Mater. Interfaces*, 2023, **15**, 49701–49711.
76 J. Feng, X. Yan, Y. Liu, H. Gao, Y. Wu, B. Su and L. Jiang, *Adv. Mater.*, 2017, **29**, 1605993.